

# JGR Solid Earth

## RESEARCH ARTICLE

10.1029/2022JB024881

### Key Points:

- Faults can be destabilized by pressure diffusion if close to hydraulic fracturing and by increase in tensile and shear stresses if distant
- Damage zone size is important when normal and shear stresses dominate the fault response to hydraulic fracturing (HF)
- Lowering injection rates does not necessarily reduce seismicity rates of faults that are stabilized by normal compressive stress during HF

### Correspondence to:

E. Maalouf and A. Yehya,  
em40@aub.edu.lb,  
ay36@aub.edu.lb

### Citation:

Yehya, A., Basbous, J., & Maalouf, E. (2022). Analysis of the hydrogeological conditions affecting fault response to nearby hydraulic fracturing. *Journal of Geophysical Research: Solid Earth*, 127, e2022JB024881. <https://doi.org/10.1029/2022JB024881>

Received 1 JUN 2022  
Accepted 28 SEP 2022

### Author Contributions:

**Conceptualization:** A. Yehya  
**Formal analysis:** A. Yehya, E. Maalouf  
**Funding acquisition:** E. Maalouf  
**Investigation:** A. Yehya, J. Basbous, E. Maalouf  
**Methodology:** A. Yehya, E. Maalouf  
**Project Administration:** A. Yehya, E. Maalouf  
**Resources:** E. Maalouf  
**Software:** A. Yehya, J. Basbous  
**Supervision:** A. Yehya, E. Maalouf  
**Validation:** A. Yehya, E. Maalouf  
**Visualization:** A. Yehya, J. Basbous, E. Maalouf  
**Writing – original draft:** A. Yehya  
**Writing – review & editing:** A. Yehya, E. Maalouf

## Analysis of the Hydrogeological Conditions Affecting Fault Response to Nearby Hydraulic Fracturing

A. Yehya<sup>1,2</sup> , J. Basbous<sup>3</sup>, and E. Maalouf<sup>4</sup> 

<sup>1</sup>Department of Civil and Environmental Engineering, Maroun Semaan Faculty of Engineering and Architecture, American University of Beirut, Beirut, Lebanon, <sup>2</sup>Harvard John A. Paulson School of Engineering and Applied Sciences, Harvard University, Cambridge, MA, USA, <sup>3</sup>Department of Geology, Faculty of Arts and Sciences, American University of Beirut, Beirut, Lebanon, <sup>4</sup>Baha and Walid Bassatne Department of Chemical Engineering and Advanced Energy, Maroun Semaan Faculty of Engineering and Architecture, American University of Beirut, Beirut, Lebanon

**Abstract** The response of critically stressed dormant faults to fluid perturbation, by oil and gas production, has been a major public concern because of its link to induced seismicity. In this paper, we study the hydrogeological factors that affect a nearby fault response, during and after hydraulic fracturing (HF) operations, evaluated by the change in Coulomb Failure Stress (CFS) and the rate of seismicity ( $R$ ) through coupling solid deformation and fluid flow. Our results show that the pore pressure increases rapidly in a fault that is close (hydraulically connected) to HF operations, which might lead to its activation when the injection rate is high. When the fault is adjacent to HF but distant from it, its shallow region is subjected to a stabilizing deformation-induced normal compressive stress and its deeper region is destabilized under extension. In this case, the fault orientation and damage zone size have a significant effect on the fault's stability and response. On the other hand, decreasing the rate of injection can either increase or decrease the CFS values depending on the fault location and the dominant stresses. Therefore, serious attention should be given to the fault position, its architecture, and the injection rate to help reduce the potential for induced seismicity from HF. Our findings are verified and confirmed using the case of the Duvernay formation in Alberta, Canada, where the reported seismic data correlate with high CFS and  $R$  values.

**Plain Language Summary** The main cause for the induced seismic events occurring during or after hydraulic fracturing (HF) operations can be attributed to fluid diffusion and/or stress changes along critically stressed dormant faults located near the operations. Different factors can affect the response of pre-existing faults to HF operations including the distance between the fault and HF operations, fault orientation, size of its damage zone, and the injection rate of HF. Based on our simulations, we conclude that when the fault is far from the operations, its shallow region (i.e., closer to HF) is subjected to a stabilizing deformation-induced compressive normal stress and its deeper region is destabilized under extension. However, for a close fault that is hydraulically connected to HF, the pore pressure increases rapidly which might lead to fault activation. Moreover, we found that decreasing the rate of injection can either increase or decrease the risk of induced seismicity depending on the fault location with respect to HF. Hence, besides avoiding fracturing rocks near faults, operators need to give serious attention to the location of faults relative to the operations, its architecture and the injection parameters to limit induce seismic events.

## 1. Introduction

Besides natural tectonic movements, earthquakes can occur due to different anthropogenic activities. These activities that cause perturbation to the underground system can alter the pressure and stresses in the nearby dormant faults. Various case studies have attempted to understand the connection of mining (Mendecki et al., 2020) and fluid production with induced seismicity (Benson et al., 2020; Davies et al., 2013; Deng et al., 2020; van Thienen-Visser et al., 2018; Zbinden et al., 2017). Meanwhile, researchers have agreed on the effect of waste fluid disposal (Healy et al., 1968), geothermal systems (Bommer et al., 2006), oil and gas production (Chang & Segall, 2016; Suckale, 2009; Villa & Singh, 2020), and hydraulic fracturing (HF) (Bao & Eaton, 2016; Brudzinski & Kozłowska, 2019; Deng et al., 2016) on the activation of dormant faults, especially that the time of some of these operations was linked to the seismic events occurring in the respective region. Unconventional oil and gas production, including HF operations, does not always induce felt seismic events of major public concern; however, under specific geological factors, major seismicity can occur even after the cessation of operations

(Rashedi & Mahani, 2016). Key parameters, such as the mechanical properties of the fault and the reservoir and the in-situ conditions, can play a significant role in increasing the probability of earthquake occurrence (Van Eijs et al., 2006; Wu et al., 2017).

In low permeability formations, conventional extraction techniques cannot economically produce oil and gas from the reservoirs. HF aims at enhancing the permeability of reservoirs and, therefore, stimulating the flow of hydrocarbons into the well (Peduzzi & Harding, 2013). In shale formations, the process is done by drilling a horizontal well followed by pressurizing a limited section of the cased well by a mixture of fluids and proppants, called HF fluid (Davis & Fisk, 2017). Seismicity can be induced during or after the high-pressure injection of fluids for formations with existing faults due to the influence of this process on the stress and strain along the fault system (Villa & Singh, 2020). Studies have concluded that most of the earthquakes induced by shale-gas stimulation are unfelt (Davies et al., 2013). However, there exists some felt seismicity, such as in Lancashire Country, UK (De Pater & Baisch, 2011), Garvin County, Oklahoma (Holland, 2013) and Horn River, Canada (Davies et al., 2013), that are proven to have a spatio-temporal correlation with HF operations.

The observed surge in the rate of seismicity in North America has been mainly attributed to the massive saltwater injection into porous formation (Frohlich, 2012). On the other hand, major earthquakes, whose magnitudes range between 2 and 6 in Alberta, CA, have been linked to the HF operations occurring in localized areas (Holland, 2013). Particularly, the seismicity in the Duvernay formation near Fox Creek, Alberta, CA started in 2014, during HF operations, and lasted till 2015, after the cessation of the operations (Schultz et al., 2017). The events are spatially and temporally correlated to the operations occurring in that area (Bao & Eaton, 2016). Knowing that the Duvernay formation is a prominent shale target in Alberta, it is vital to answer questions that justify the occurrence of the seismic events there.

There are two major physical mechanisms to trigger an earthquake during fluid injection. The first mechanism is the pore pressure diffusion along permeable fractures or along the damage zones of existing faults or cores, particularly if the fault has been recently active. This is mostly the case for the induced seismicity in the United States that occurred due to the injection of massive saltwater volumes into porous formations; the pore fluid pressure can diffuse for long distances until it reaches a critically stressed fault (Ellsworth, 2013; Galloway et al., 2018; Schultz et al., 2014). The second mechanism is caused by the stress changes due to the solid matrix response to injection or production (Ellsworth, 2013). Generally, there are two major factors that help nucleate an earthquake (Galloway et al., 2018): (a) the presence of a nearly critical slip-oriented fault and (b) a mean to induce stress perturbation on the fault past the critical condition. The first factor must have existed for an induced seismic event to occur (McClure & Horne, 2014). The ambiguity lies in the second factor which can be triggered by different, possibly man-induced, means. The perturbation can occur either by pore pressure diffusion that is transmitted along the damage zone (Yehya et al., 2018) or poroelastically through an impermeable rock matrix (Galloway et al., 2018) reactivating the existing faults and, therefore, releasing their stored strain energy (Walsh & Zoback, 2015). Another mechanism is the deflection of the propagating hydraulic fracture into fault planes, which are common in the field (Gudmundsson, 2011). When the hydraulic fracture enters the fault plane, the flow is controlled by the Cubic law. Whether or not the hydraulic fracture deflects into the fault and follows the fault plane depends on various mechanical factors (Gudmundsson, 2022). During HF, the change in pore pressure alone is unlikely to induce felt seismic events of major public concern (Bao & Eaton, 2016; Deng et al., 2016) because the pore pressure would require time to diffuse along the fault and would experience changes after hours of injection, especially if the hydraulic fractures are not directly connected to the damage zone of the fault. However, the shear and normal stresses in hydraulically fractured poroelastic medium vary instantly and significantly. Consequently, both the deformation of porous solid material and the change in pore fluid pressure (also known as poroelastic effects (Rice & Cleary, 1976)), affect the steady state of the fault (Deng et al., 2016).

Fisher and Warpinski (2012) presented a review of field data of different wells located at depths spanning from 900 to 4,300 m. The review shows that the aforementioned mechanisms can trigger the earthquake either at the source of the stress or pressure perturbation or deep below and away from the source. Besides, events can occur shortly after the anthropogenic activity begins or after it has been ceased. However, there exist certain hydrogeological conditions that facilitate fault reactivation (Witherspoon & Gale, 1977); these conditions need to be studied and analyzed while taking into consideration the importance of the two-way coupling between solid deformation and fluid flow. In this work, we explore the hydrogeological factors and perturbation mechanisms

affecting faults' response during and/or after HF operations. We mainly focus on the location of the fault, its orientation, the presence of a hydraulic connection between the HF zone and the faults, and the width of the damage zones. We also investigate the effect of the injection rate. To assess the fault response, we estimate the change in the Coulomb Failure Stress (CFS) along a critically stressed fault that is located near the HF operations using a two-dimensional finite element poroelastic model on COMSOL Multiphysics. This approach has been implemented previously to study the stability of the faults associated with CO<sub>2</sub> injection (Rutqvist et al., 2007; Vilarrasa et al., 2016), water-injection (Rutqvist, 2011; Yehya et al., 2018), reservoir impoundment (Basbous et al., 2022) and HF (Rutqvist et al., 2013, 2015). In the second part of the study, we consider the case study of the Duvernay formation in Alberta, Western Canada where seismic events were reported during and after operations, to relate the fault response to real seismic data. The variations of the CFS along the two critically stressed faults are analyzed and compared to the seismic events obtained from the observational data from December 2014 to March 2015 (Bao & Eaton, 2016).

The paper is divided as follows. Section 2 describes the method used, the geology of the formations, and the model construction. Section 3 explains the linear poroelastic model and the governing equations. In Section 4, we present synthetic cases to independently discuss the effect of different geometrical and hydrological factors on fault activation. In Section 5, we verify our findings using the study case of Alberta, CA. Finally, Section 6 concludes on the main outcomes and recommendations drawn from the work.

## 2. Materials and Methods

We couple fluid flow and solid deformation to account for the poroelastic behavior and estimate the change in the CFS. The accuracy of coupled models for fluid flow and deformation depends on how the coupling is realized (Beck et al., 2020; Blanco-Martin et al., 2017; Both et al., 2018; Kim, 2010; Kim et al., 2012).

The equations of fluid flow and solid mechanics are fully coupled using COMSOL Multiphysics. There are two approaches to solve the multi-physics problem on COMSOL Multiphysics: the fully coupled and the sequential or segregated approaches. The fully coupled approach forms a single large system of equations that solve for all of the fields and includes all of the couplings at once, within a single iteration. On the other hand, in the segregated approach, the problem is subdivided into several segregated steps. These individual segregated steps are smaller than the full system of equations that are formed with the fully coupled approach. The segregated steps are then solved sequentially. Regardless of the approach, the solution is approached by each iteration until gradually converging to the solution. The fully coupled approach often converges more robustly and in fewer iterations as compared to the segregated approach. However, each iteration will require relatively more memory and time to solve. The sequential approach can be faster but introduces different kinds of errors especially when the sequential scheme is not iterative (Beck et al., 2020). Hence, it is useful in 3D, however, the 2D assumption in our model allows us to use the fully coupled approach, which gives high accuracy despite the higher computational time. Consequently, we use a 2D plane strain model with a geometry inspired by the Duvernay formation case in Alberta, Canada, where induced seismicity is associated with HF operations.

The entire domain is 10 km × 10 km and is divided into three layers. The shale reservoir is 400 m thick, the overburden layer is 3.2 km thick and the crystalline basement is 6 km thick as depicted in Figure 1. A critically stressed fault is added near the HF operations. Table 1 summarizes the different cases studied where we varied the injection rate (of the HF operations), the orientation and location of the fault, and the width of the damage zone. The simulation is simplified to a 2D model because HF operations occur around a horizontal well and affect the formation properties of a vertical planar region of relatively small width with respect to the domain. Moreover, the main fractures generated by the HF operations propagate in the vertical plane (Khadijeh et al., 2022). Therefore, we consider a cross section that passes through the horizontal well for the 2D model shown in Figure 1. In order to simulate the stages of the HF operations, 15 injection points that are separated by a distance of 70 m are added at a depth of 3.4 km within the HF zone (Figure 1). The permeability of the HF zone is higher than the host rock due to HF and is considered to increase instantly during the operation. The fault has a fault core of low permeability (order of 10<sup>-17</sup> m<sup>2</sup>), and boarding damage zones of higher permeability (order of 10<sup>-14</sup> m<sup>2</sup>) (Mitchell & Faulkner, 2009). The fault is considered as a dormant fault (inactive), however, when active, there will be an increase in the fault core permeability. This is not considered in our model. The injection points are activated one after the other by injecting 9 m<sup>3</sup>/min water per mass source for 5 hr followed by 4 hr of zero-injection phase.

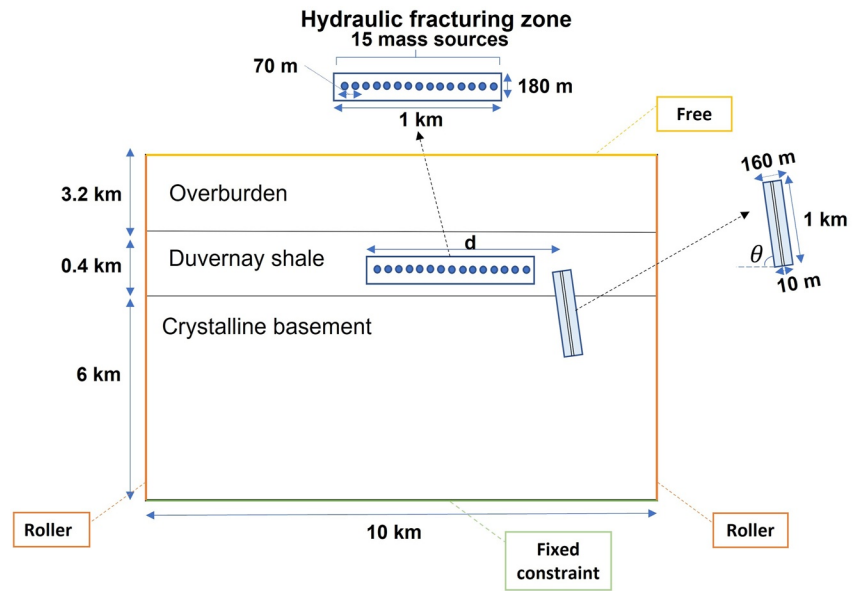


Figure 1. A 2D schema showing the geological formation and the geometry of the hydraulic fracturing zone and the fault.

### 3. Theory and Calculations

#### 3.1. Poroelastic Model and Governing Equations

##### 3.1.1. Coulomb Stress Changes

Generally, the change in CFS expresses the failure criterion to initiate rupture:

$$\Delta CFS = \Delta \tau + f(\Delta \sigma_n + \Delta p) \quad (1)$$

where  $f$  is coefficient of friction, taken equal to 0.6,  $\Delta \tau$  is the change in the shear stress,  $\Delta \sigma_n$  is the change applied normal stress (positive for extension) and  $\Delta p$  is the change in pore pressure or the change in fluid pressure along the fault plane (Gudmundsson, 2011). Any natural or anthropogenic activity that alters the shear stress, normal stress or pore pressure can bring the fault to failure and, therefore, induce an earthquake. Hence, for a critically stressed fault, as the case of most dormant faults in the subsurface, any positive change in the CFS affects the fault's response to the perturbation and could lead to fault slip.

##### 3.1.2. Coupled Poroelastic Model

The coupled poroelastic model states that the change in pore pressure affects the stresses and strains (fluid-to-solid coupling) and, similarly, any change in the poroelastic stresses can lead to the variation of pore pressure (solid-to-fluid) (Biot, 1941; Rice & Cleary, 1976; Wang, 2000).

The equilibrium equation, under quasi-static condition, and no additional body forces gives:

$$\nabla \cdot \sigma = 0 \quad (2)$$

The constitutive equation of the solid matrix when pore fluid is under pressure, with the approximation of elastic isotropy, is given by:

$$G \nabla^2 \mathbf{r} + \frac{G}{1-2\nu} \nabla \epsilon - \alpha \nabla p = 0 \quad (3)$$

Table 1  
Geometrical and Injection Parameters Used in the Synthetic Cases

Studied cases	Injection rate (m <sup>3</sup> /min)	Dip (°)	Distance from HFZ; $d$ (m)	Intersection with HFZ	Damage zone width Wd (m)
Case 1	9	90	600 (middle of HFZ)	Yes	160
Case 2	9	90	1,600 (distant)	No	160
Case 3	9	90	2,200 (far)	No	160
Case 4	9	90	600	No	160
Case 5	9	80	600	Yes	160
Case 6	9	70	600	Yes	160
Case 7	9	80	1,800	No	160
Case 8	9	90	1,800	No	160
Case 9	9	70	1,800	No	160
Case 10	9	90	600	Yes	40
Case 11	9	90	1,600	No	40
Case 12	9	90	600	Yes	80
Case 13	9	90	1,600	No	80
Case 14	3	90	600	Yes	160
Case 15	5	90	600	Yes	160
Case 16	3	90	1,600	No	160
Case 17	5	90	1,600	No	160

**Table 2**  
*Porosity and Permeability of the Geological Components Used in the Numerical Models*

Component	Permeability (m <sup>2</sup> )	Porosity (-)	Reference
Duvernay shale	1.5 E - 19	0.065	(Kleiner & Aniekwe, 2019)
Crystalline basement	10 <sup>-21</sup>	0.01	(Stober & Bucher, 2014)
Hydraulic fracturing zone	10 <sup>-16</sup>	0.1	(Rodríguez-pradilla, 2018)
Damage zones	10 <sup>-14</sup>	0.1	(Yehya et al., 2018)
Fault core	10 <sup>-17</sup>	0.015	

where  $\mathbf{r}$  is the displacement vector,  $G$  is the shear modulus,  $\nu$  is Poisson's ratio,  $\epsilon$  is the volumetric strain,  $\alpha$  is Biot-Willis coefficient and  $\nabla p$  is the applied pressure gradient.

The fluid equation, derived from the conservation of mass, requires that:

$$\frac{\partial}{\partial t}(\varnothing\rho) + \nabla \cdot (\rho\mathbf{u}) = Q_m \quad (4)$$

where  $\rho$  is the density of the fluid,  $\varnothing$  is the porosity of the medium, and  $Q_m$  is the fluid mass source.

Fluid flow in a poroelastic medium can be described by Darcy's Law where Darcy's velocity,  $\mathbf{u}$ , is expressed in terms of the permeability of the medium,  $\kappa$ , fluid viscosity,  $\mu$ , and the difference in elevation,  $\nabla z$ :

$$\mathbf{u} = -\frac{\kappa}{\mu} (\nabla p + \rho g \nabla z) \quad (5)$$

Furthermore, the poroelastic storage coefficient,  $S$ , is given by:

$$\frac{\partial}{\partial t}(\varnothing\rho) = \rho S \frac{\partial \rho}{\partial t} \quad (6)$$

Then, the mass conservation equation can be re-written as:

$$\rho S \frac{\partial \rho}{\partial t} + \nabla \cdot (\rho\mathbf{u}) = Q_m = -\rho\alpha \frac{\partial \epsilon}{\partial t} \quad (7)$$

The negative sign in the mass source term refers to the effect of the increase of the rate of change of the volumetric strain,  $\partial \epsilon / \partial t$ . As this term increases, there is more space for the fluid to diffuse.

### 3.2. Initial and Boundary Conditions

For the initial conditions, the displacement vector is null, and the pore pressure is at hydrostatic conditions. Thus, the calculated pore pressure is the excess pressure above the hydrostatic value. As for the boundary conditions for the solid matrix, we use shear-free but impenetrable boundaries for the side and bottom boundaries described as,

$$\mathbf{n} \cdot \mathbf{u} = 0, \mathbf{n} \times (\boldsymbol{\sigma} \cdot \mathbf{n}) = 0 \quad (8)$$

where  $\mathbf{u}$  is the displacement of the solid matrix, and  $\boldsymbol{\sigma}$  is the stress tensor.

**Table 3**  
*Linear Elastic Properties of the Geological Components Used in the Numerical Models*

Component	Young's modulus (GPa)	Poisson's ratio (-)	Density (kg/m <sup>3</sup> )	Reference
Duvernay shale	75	0.25	2,700	(Zhao, 2018)
Crystalline basement	60	0.2	2,750	
Damage zones	25	0.25	2,700	(Gudmundsson, 2004)
Fault core	5	0.25	2,700	

**Table 4**  
*Poroelastic Property of the Geological Components Used in the Numerical Models*

Component	Biot-Willis coefficient (–)	Reference
Duvernay shale	0.79	(Fan et al., 2019)
Crystalline basement	0.44	

The top side is free to move in any direction (traction-free) (Fan et al., 2016; Segall & Lu, 2015). For the fluid flow, we assume a zero normal component of the fluid mass flux as,

$$-\mathbf{n} \cdot (\rho \mathbf{v}_f) = 0 \quad (9)$$

where  $\mathbf{n}$  is the normal vector pointing outward,  $\rho$  is the fluid density, and  $\mathbf{v}_f$  is the fluid velocity. The boundaries are chosen far enough from the fluid perturbation (i.e., injection site) by enlarging the size of the studied domain. A sensitivity analysis on the location of the boundary was performed to ensure that the boundary conditions on it does not affect the results.

Tables 2–4 describe the hydraulic, linear elastic and poroelastic properties of the different geological components, respectively, while Table 5 describes the fluid properties used in the numerical models.

### 3.3. Rate of Seismicity

To evaluate the potential for induced seismicity, we calculate the rate of seismicity (Chang & Yoon, 2018; Segall & Lu, 2015). Dieterich (1994) developed a seismicity rate model, governed by rate and state friction, to relate the rate of earthquake nucleation to changes in coulomb stress. In the absence of any stress perturbation, the rate of seismicity will remain constant with time. When stress perturbation occurs, an increase in this rate is expected. The rate of seismicity  $R$  can be calculated relative to a background stressing rate by:

$$\frac{dR}{dt} = \frac{R}{t_a} \left( \frac{\dot{\tau}}{\dot{\tau}_0} - R \right) \quad (10)$$

$\dot{\tau}_0$  being the background stressing rate,  $\dot{\tau}$  Coulomb stressing rate estimated from the model as the rate of change in the overall change in Coulomb stress, and  $t_a \equiv a\bar{\sigma}/\dot{\tau}_0$  is the characteristic relaxation time, where  $a$  is the constitutive parameter in the rate state friction law quantifying the direct effect on slip. In this study,  $\bar{\sigma}$  is the average vertical effective normal stress and is equal to 71.7 MPa,  $\dot{\tau}_0 = 0.001$  MPa/year corresponds to a cumulative stress drop of 1 MPa every 1,000 years, and  $a = 0.003$  (Chang & Yoon, 2018; Segall & Lu, 2015). Therefore, the resulting characteristic relaxation time is  $t_a = 215$  years. However, when there is an overpressure beyond the hydrostatic pressure, as it is the case in Alberta (Eaton & Schultz, 2018), the time  $t_a$  will decrease and its effect on  $R$  is highlighted in Section 5. The initial value of  $R$  is 1 and  $R$  returns to its initial value when time  $t \gg t_a$  (see Equation 10).

## 4. Effect of Hydrogeological Factors on Fault Response

In this section, we discuss the possible hydrogeological factors that affect a fault response to HF, which can lead to triggering seismicity. We evaluate and analyze the effect of fault location, fault orientation, intersection between the HF zone and the fault damage zones, the width of the bordering damage zones, and the injection rate on the change of CFS along the critically stressed fault. Then, we estimate the rate of seismicity on two chosen points of the fault (shallow and deep). The change in CFS, pore pressure and the overall Coulomb stresses are evaluated during and after the HF operations. The stress calculated is the total stress ( $\sigma_{total}$ ) that is estimated from the effective stress ( $\sigma_{eff}$ ) calculated by COMSOL Multiphysics as  $\sigma_{total} = \sigma_{eff} \pm \alpha p$ .

**Table 5**  
*Fluid Properties Used in the Numerical Models*

Fluid properties	Value
Density (kg/m <sup>3</sup> )	1,000
Dynamic viscosity (Pa · s)	0.0004
Compressibility (1/Pa)	4E – 10

### 4.1. Effect of Fault Location

We vary the distance ( $d$  in Figure 1) between the fault and the HF operations, to assess its effect on the CFS and  $R$  values. The different location of the fault are given in cases 1 through 4 in Table 1. The following subsections illustrate the results obtained for each case. We conclude from the observations that the fault response falls within three categories depending on the value of  $d$ . The first is when the fault is below the HF region and is hydraulically connected

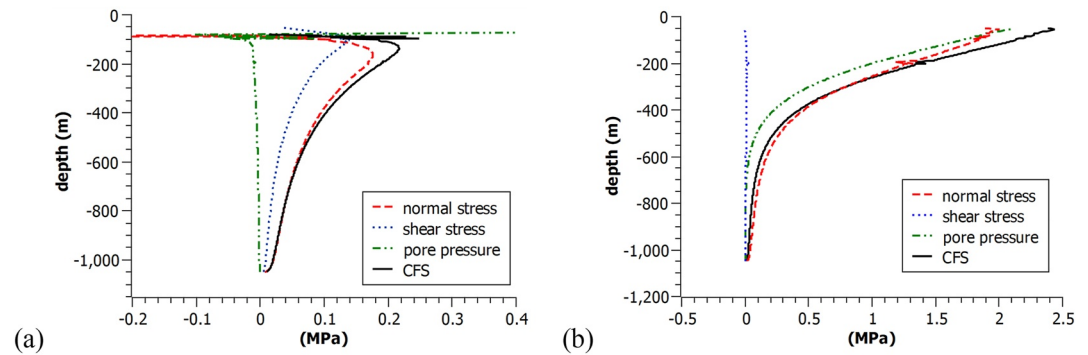


**Figure 2.** Normal and shear stresses, pore pressure, and Coulomb Failure Stress values measured on the vertical fault (a) during injection (at  $t = 90$  hr), and (b) after injection ends (at  $t = 2,000$  hr) for case 1 ( $d = 600$  m).

to it (i.e., for  $0 < d < 1$  km). The second is when the fault is to the right of HF zone and slightly distant (i.e.,  $1 \text{ km} < d < 2.2$  km). And the third is when  $d > 2.2$  km.

#### 4.1.1. Case 1, $d = 600$ m

Figure 2 shows that when  $d = 600$  m, the dominant mechanism affecting the CFS is pore pressure diffusion. The pore pressure is high in the shallower fault region and it diffuses deeper as time passes (Figure 2b). Hence, the CFS values increase after the end of HF operations as seen in Figure 3a. The CFS values in the shallow part increase slightly during HF, then increase sharply after the end of injection and continue to increase until the CFS stabilizes. In deeper regions, the CFS values continue to increase as pore pressure diffuses along the fault. Accordingly, the rate of seismicity increases for the shallower region near the end of HF operations (end of injection), then it starts to decrease as the rate of change of CFS decreases (Figure 3b). In the deep regions, the rate of seismicity keeps increasing after the HF operation stops and continues to increase until the pore pressure perturbation diminishes (Figure 3b).

#### 4.1.2. Case 2, $d = 1,600$ m

Figure 4 shows that when  $d = 1,600$  m, the response of the fault is caused by an indirect fluid pore pressure effect. The injected fluid at high pressure causes an increase in the compressive normal stress on the shallower region of the fault (Figure 4). This will help stabilize the shallow part of fault and decrease the overall change in CFS. The shear stress increases in the middle region of the fault causing an increase in the CFS to values beyond 0.01 MPa, which might lead to fault destabilization. Figure 5a shows that the CFS values do not increase significantly in the deeper region after the cessation of the HF operations, signifying a decrease in the rate of seismicity (Figure 5b). We conclude that induced seismicity is expected to occur only during the HF operations if the fault is located in the region where  $1 \text{ km} < d < 2.2$  km.

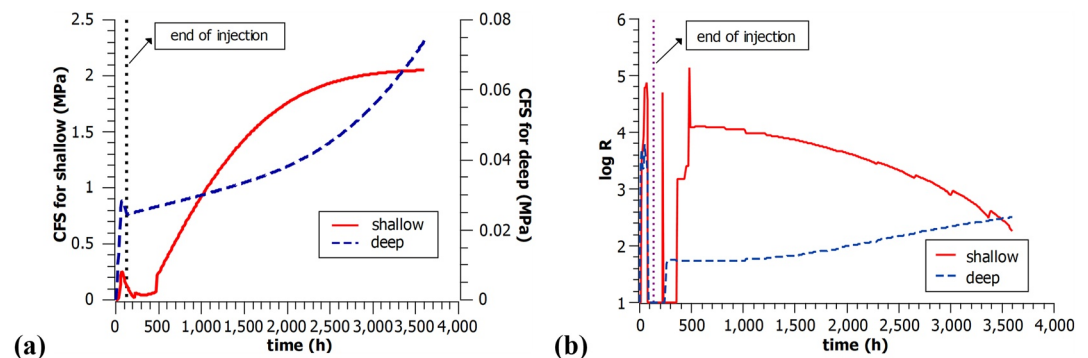


**Figure 3.** The variation with time of the (a) Coulomb Failure Stress and (b)  $\log R$ , for a shallow point ( $h = 0.15$  km) and a deep point on the fault ( $h = 0.9$  km) for Case 1 ( $d = 600$  m). The vertical dotted line represents time at end of injection (120 hr).

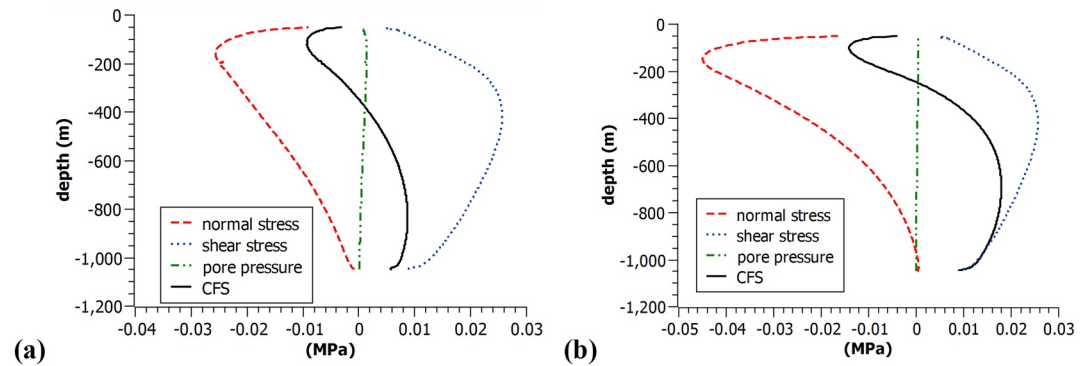


**Figure 4.** Normal and shear stresses, pore pressure, and Coulomb Failure Stress values on the vertical fault (a) during injection (at  $t = 90$  hr) and (b) after injection ends (at  $t = 2,000$  hr) for Case 2 ( $d = 1,600$  m).

#### 4.1.3. Case 3, $d = 2,200$ m

When the fault is at a distance  $d > 2,200$  m, the HF operations have a minimal effect on the fault's response, which is evident from the comparison between the CFS values between  $d = 1,400$  m,  $d = 2,100$  m, and  $d = 2,200$  m (Case 3) illustrated in Figure 6. Between  $d = 2,100$  m and  $d = 2,200$  m, a transition occurred from a positive to a near zero or negative CFS values, which indicates no risk for induced seismicity.

#### 4.1.4. Case 4, No Intersection Between the Fault and the HF Region

We investigate the response of the fault located below the HF zone when no hydraulic connection exists between them. Figure 7a shows that the CFS values decrease in the absence of intersection, which is caused by the significant decrease in the pore pressure values. Furthermore, Figure 7b shows that the mechanism of fault activation will shift from pore pressure diffusion when a hydraulic connection exists (e.g., Cases 1 through 3) to being affected by an increase in tensile and shear stresses on the fault in the absence of hydraulic connection.

We conclude that the fault location with respect to HF affects the fault response and plays an important role in the mechanism of fault activation by induced seismicity. This observation, has important implications on the strategy of injection that can be tailored according to the faults location and the mechanism that affects the faults, hence, reducing the risk for induced seismic events.

The effect of injection rate is further examined in Section 4.4. Opposing effects can be obtained based on the location, or more precisely based on the fault's response and activation mechanism.

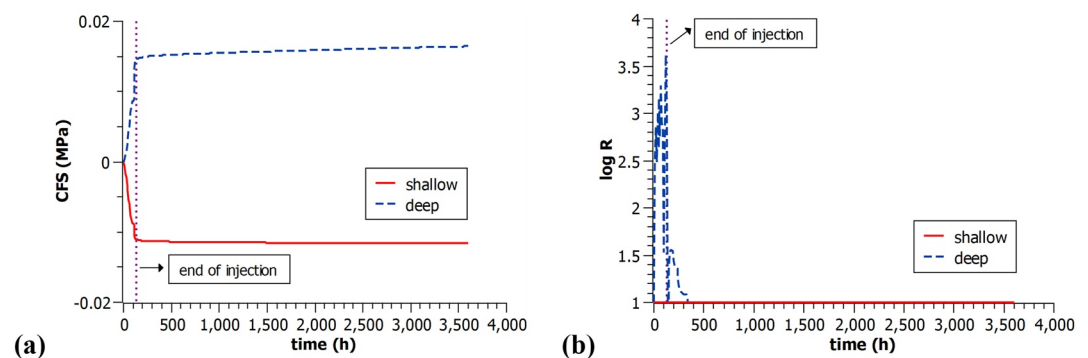


**Figure 5.** The variation with time of the (a) Coulomb Failure Stress and (b)  $\log R$ , for a shallow point ( $h = 0.15$  km) and a deep point on the fault ( $h = 0.9$  km) for Case 2 ( $d = 1,600$  m). The vertical dotted line represents time at end of injection (120 hr).

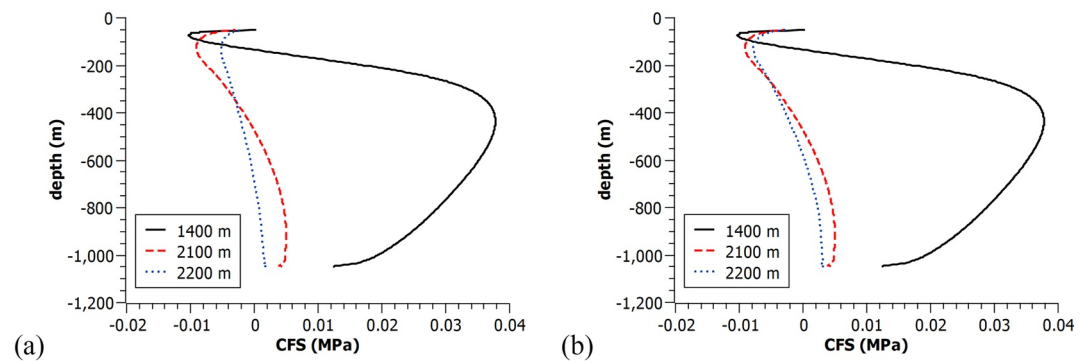


**Figure 6.** Coulomb Failure Stress values along the vertical fault for different values of  $d$ , (a) during injection (at  $t = 90$  hr) and (b) after injection ends (at  $t = 2,000$  hr).

#### 4.2. Effect of Fault Orientation

We investigate the effect of fault orientation on the response of the fault during and after HF operations. Note that the attitude (strike and dip) of the fault has strong effects on the likelihood of a propagating hydraulic fracture to deflect when meeting a fault (Gudmundsson, 2022). The fault strike is considered to be  $90^\circ$  and the fault dip,  $\theta$ , is variable as per cases 4–9 in Table 1. The normal vector on the fault is  $\mathbf{n}$  ( $n_1 = \sin \theta, n_2 = 0$ ). The normal stress is calculated as  $\sigma_n = \sigma_{11}n_1^2$  and the shear stress as  $\tau = (\sigma_{11}^2n_1^2 + \sigma_{12}^2n_1^2 - \sigma_{11}^4)^{1/2}$ , where  $\sigma_{11}$  and  $\sigma_{12}$  are the components of the stress tensor.

We notice from Figure 8a that for the close fault (i.e.,  $0 < d < 1$  km; cases 1, 5, and 6), where pore pressure diffusion is the dominant mechanism for fault activation, the effect of fault orientation is minimal as long as the intersection with HF zone is maintained. However, Figure 8b shows that when  $1 \text{ km} < d < 2.2$  km (cases 7, 8, and 9), the CFS values are highly affected by the fault orientation and this is due the increase in compressive normal stress and shear stress on the fault.

#### 4.3. Effect of the Fault Damage Zone

The fault damage zone is a region surrounding the fault core that includes micro-cracks which induce a higher permeability and reduced mechanical properties. Damage zones are reported to act as conduits for fluids which enhance pore pressure diffusion, as opposed to the fault core that is cemented and have low permeability. The size of damage zone and its permeability is affected by coseismic damage (Yang et al., 2021) and interseismic healing processes (Yehya & Rice, 2020). Narrow damage zones exist in mature faults that have undergone healing or strain localization. Wide damage zones exist mostly in active faults. The effect of the width of the damage zone ( $W_d$ ) on the fault response depends on the nature of stress perturbation affecting the fault. Following the results

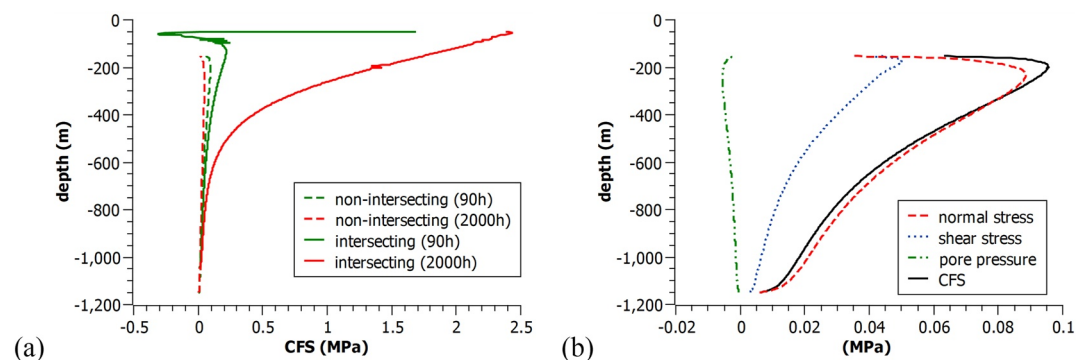


**Figure 7.** (a) Comparison of the Coulomb Failure Stress (CFS) values along the vertical fault for cases 1 and 4 at 90 and 200 hr. (b) Normal and shear stresses, pore pressure, and CFS values along the vertical fault for case 4 (no intersection with the hydraulic fracturing zone) when  $t = 90$  hr.

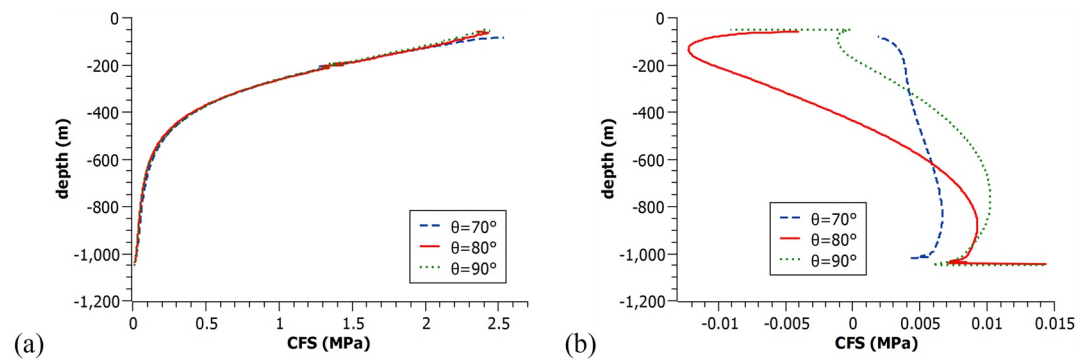


**Figure 8.** Coulomb Failure Stress values measured at  $t = 2,000$  hr for different fault orientations  $\theta$ , for (a) cases 1, 5, and 6 (where  $0 < d < 1$  km) and (b) cases 7, 8, and 9 (where  $1 \text{ km} < d < 2.2$  km).

of Section 4.1, it was found that the location of the fault affects its stability and stress perturbation. Hence, the size of the damage zone affects the faults response differently for different fault locations ( $d$ ). For the case of the close fault (i.e.,  $0 < d < 1$  km), the width of the damage zone does not significantly affect the CFS values as seen in Figure 9a. It is sufficient to have a conduit (i.e., a high permeability region) of a small size to allow pressure diffusion along the fault.

Figure 9b shows that when the fault is distant that is, when the dominant mechanism of fault activation is the increase in tensile and shear stresses (see Section 4.1), the effect of the damage zone size on the CFS is more evident. As the size of the damage zone decreases, the shear stress build up is higher in the deeper region of the fault with a higher tensile normal stress. The compressive normal stress acting on the shallower region of the fault is due to the normal deformation caused by the HF loading. In the case of a thinner damage zone, the average modulus of elasticity is higher resulting in a higher compressive normal stress, and thus, in lower CFS values and more stabilization in the shallow region as shown in Figure 9b. When the damage zone width increases, the average modulus of elasticity decreases leading to lower deformation-induced compressive normal stress in the shallower region and higher destabilizing tensile and shear stress in the deeper regions of the fault. This is an interesting observation on the role of the damage zones and how it is different depending on the loading state of the fault caused by HF. One scenario where a higher damage zone width increases the CFS values in the shallow part of the well is when  $d$  is slightly greater than 1 km and the larger damage zone allows a lateral hydraulic connectivity between the fault and the HF zone.

#### 4.4. Effect of Injection Rate ( $q$ )

The effect of the injection rate on the fault is determined by the location of the fault ( $d$ ), or more precisely, by the response of the fault and the dominant mechanism that leads to failure.

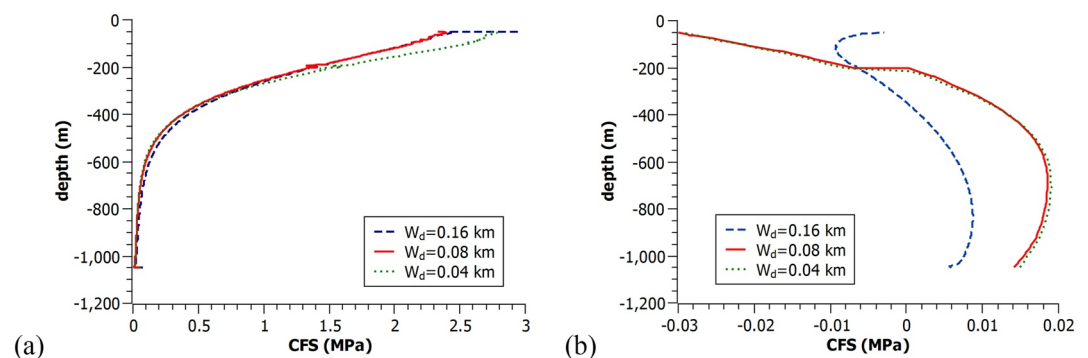


**Figure 9.** Coulomb Failure Stress values for different fault damage zone thicknesses ( $W_d$ ) obtained at  $t = 2,000$  hr (a) for cases 1, 10, and 12 (where  $0 < d < 1$  km) and (b) for cases 2, 11, and 13 (where  $1 \text{ km} < d < 2.2$  km).

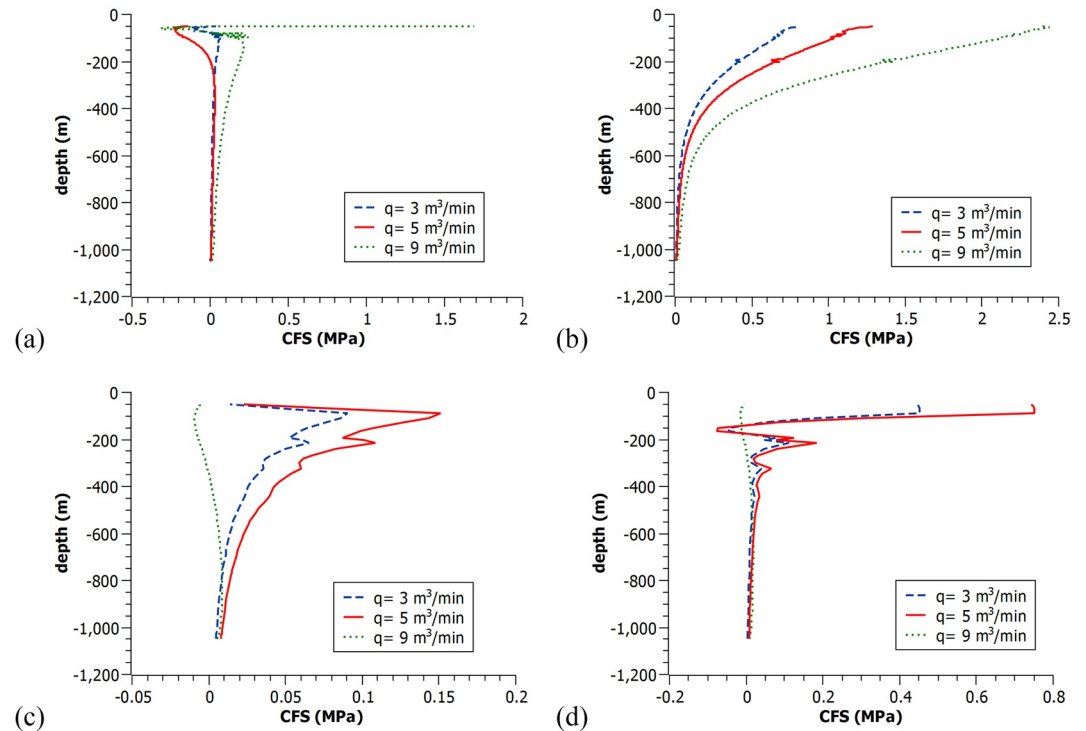


**Figure 10.** Coulomb Failure Stress values for various injection rates for cases 1, 14, and 15 (where  $0 < d < 1$  km) (a) at  $t = 90$  hr, and (b) at  $t = 2,000$  h, and for cases 1, 16, and 17 ( $1 \text{ km} < d < 2.2$  km) (c) at  $t = 90$  hr, and (d) at  $t = 2,000$  hr.

When  $0 < d < 1$  km (Figures 10a and 10b), the CFS increases when the injection rate increases because of the increase in pore pressure. The pore pressure is the dominant mechanism for fault activation for these values of  $d$ , therefore, decreasing the injection rate would lead to a reduction in CFS. So, adopting a lower injection rate can prevent induced seismicity for a fault that is located below the HF operations and that is hydraulically connected to it.

When  $1 < d < 2.2$  km (Figures 10c and 10d), the high injection rate creates a high deformation-induced normal compressive stress on the shallow region of the fault, and thus, stabilizes it. However, as the injection rate is reduced, the normal compressive stress is no longer significant and does not dominate the overall Coulomb stress change. Hence, the shallow part of the fault will be destabilized during HF for low injection rates. It was noticed that for the studied settings there is an injection rate threshold beyond which the effect of HF on the fault goes from creating a normal tensile stress with high shear stress (for  $q = 3$  and  $5 \text{ m}^3/\text{min}$ ) to creating a compressive normal stress (for  $q = 9 \text{ m}^3/\text{min}$ ) (Figure 11). These findings have important implications on the choice of the injection strategy as it

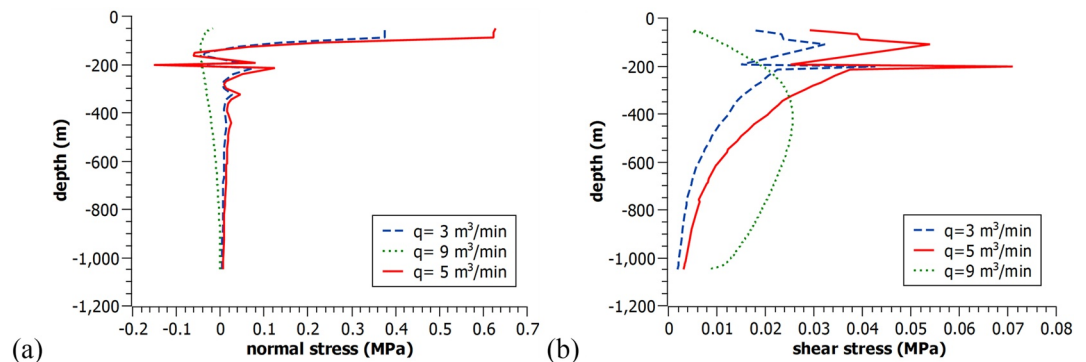


**Figure 11.** Normal and shear stresses for various injection rates for cases 1, 16, 17 (a) for  $t = 90$  hr (during injection) and (b) for  $t = 2,000$  hr (after injection).

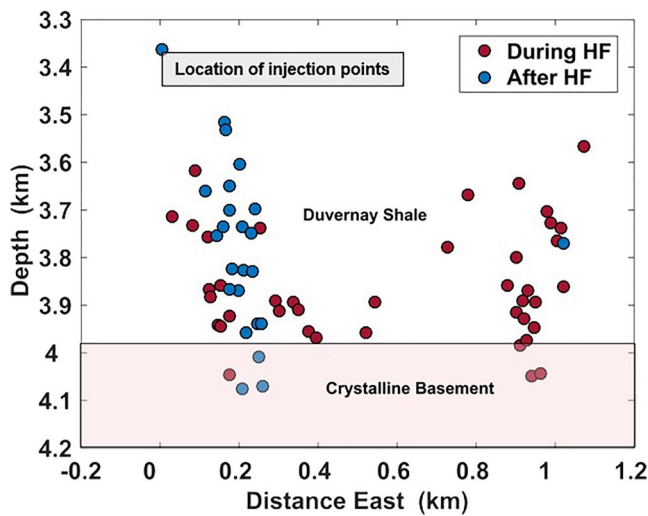


**Figure 12.** Cross section of a cluster showing the two strands of the fault system in the Duvernay formation (reproduced from Bao & Eaton, 2016).

will depend on the known fault location and the fault response. We conclude that to avoid seismicity in a fault below the HF zone, the injection rate should be reduced. However, to avoid seismicity in a moderately distant fault, the injection rate should be high enough to create a normal compressive stress that can stabilize the upper region with a tensile and shear stresses small enough to avoid destabilizing the lower region. An optimum injection strategy based on different factors needs a more extensive study and merits more investigation. This can be done in a perspective work, which does not only look at the injection rates but also injection volumes and preserving the hydraulic energy to ensure efficient results of HF and its permeability increase.

## 5. Study Case: Induced Seismicity in Alberta, CA

We verify the results obtained in Section 4 by modeling the HF operation conducted on the Duvernay formation in Alberta, CA, where a sequence of seismic events occurred between end of 2014 and early 2015.

### 5.1. The Duvernay Formation

The Duvernay is an Upper Devonian mud rock containing significant quartz and limestone which makes it an attractive Shale gas target. Lithologically, the Duvernay formation is composed of laminated bituminous shale, calcareous shale, and dense argillaceous limestone. It contains 443 trillion cubic feet of Natural Gas, 11.3 billion barrels of Natural Gas Liquids and 61.7 billion barrels of oil (Preston et al., 2016).

Irregular seismicity has been observed in the Duvernay formation in Alberta, CA since December 2013 (Bao & Eaton, 2016). These events have been spatially and temporally correlated with the HF activities occurring in the Upper Devonian Duvernay formation (Schultz et al., 2015). The link between these events and fracking operations was controversial at that time, where some authors (Atkinson et al., 2016) correlated the events with the saltwater disposal in Mississippian Debolt formation; however, the amount of water injected was not enough to have induced the observed seismic events (McGarr, 2014).

Seismic events were observed at the end of 2014 and early January 2015 during HF operations in the Duvernay formation. Even after the cessation of the operations, three sequences were also detected: S1 (January 10 till 31 January 2015), S2 (February 1 till 18 February 2015) and S3 (March 9 till 31 March 2015). Each sequence is characterized by a set of events of increasing magnitude followed by a break. In this work, we analyze the three sequences as one post treatment sequence that we refer to as after HF. The distribution of the seismic events in that cluster outlines a strike-slip system of two faults near the HF operations and with similar orientation (Bao

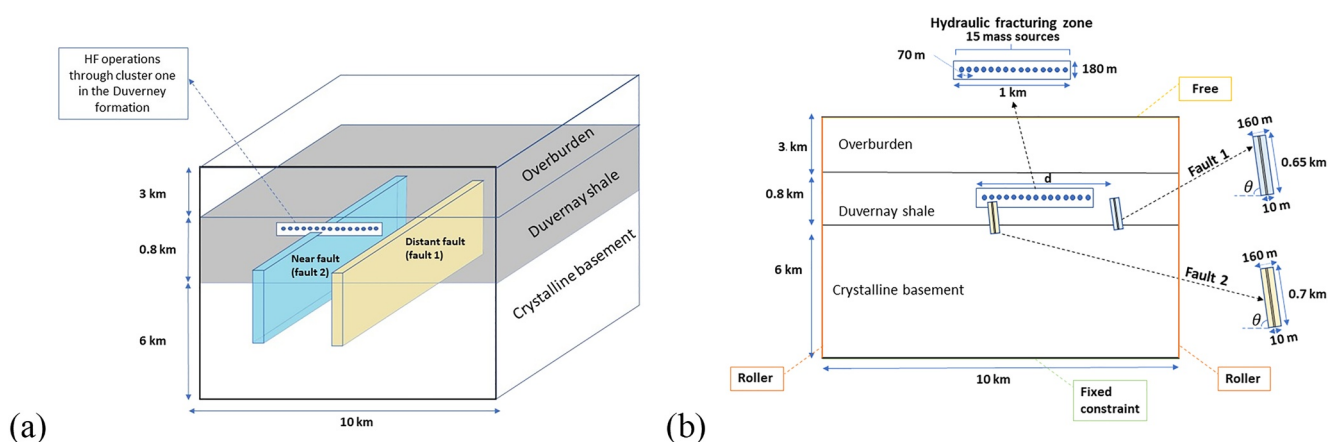


**Figure 13.** (a) 3D schematic showing the geological settings of the Alberta case, and (b) the simulated 2D cross-section showing the faults, the hydraulic fracturing injection sources, and the solid mechanics boundary conditions.

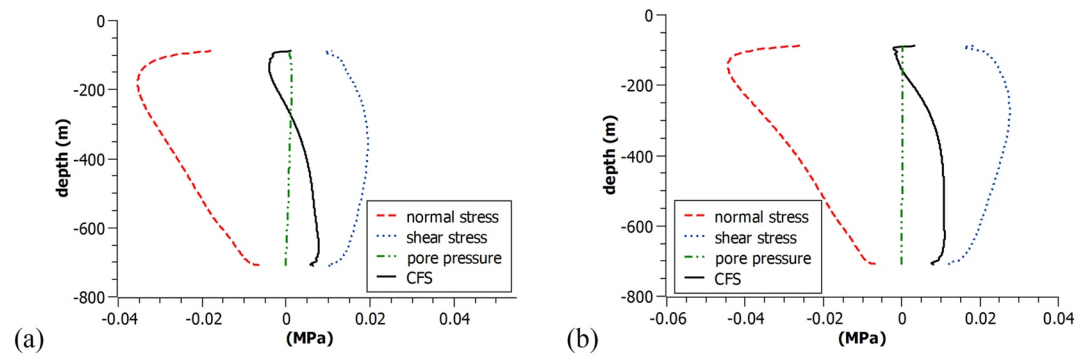


**Figure 14.** Normal and shear stresses, pore pressure, and Coulomb Failure Stress values on Fault 1 (distant) for the Alberta case: (a) during injection (at  $t = 90$ hr), and (b) after injection ends (at  $t = 2,000$  hr).

& Eaton, 2016) as shown in Figure 12. The faults extend from the injection zone within the Duvernay formation into the crystalline basement as shown in the schematic of Figure 13. The injection points, at a depth of 3.4 km (Zhao, 2018), are activated one after the other by injecting  $9 \text{ m}^3/\text{min}$  water per mass source for 5 hr followed by 4 hr of zero-injection phase.

In the simulations, we explain the correlation between the numerically estimated positive CFS and rate of seismicity  $R$  values describing the fault response and the observed seismic data.

Fault 2 (see Figure 13) is located at  $d < 1$  km, therefore it is expected to be mainly affected by pore pressure diffusion caused by the HF operations (based on the results of Section 4). This leads to more destabilization of its shallower section. However, Fault 1 is located at  $d > 1$  km, hence its shallow region is expected to be under compression and is stabilized while smaller part of its deeper section is destabilized due to a lower compressive normal stress and higher shear stress (Figure 14).

This expected behavior is confirmed by the simulation results illustrated in Figures 14–17. The shallow region of Fault 1 (the distant fault) shows a stabilized behavior during HF and the deeper part is destabilized. When compared with the seismic events of Figure 12, we observe that there is a match between the high CFS values and the events. This is further confirmed by the values of  $\log R$  shown in Figure 15a where  $\log R$  is low during the HF operations (time  $< 131$  hr) for the shallow part of the fault, which correlates with the absence of seismicity for this time interval. The  $\log R$  values slightly increase after HF, and interestingly there is one reported event after HF in this region (Figure 12). In the deep part of the fault, the values of  $\log R$  increase during HF and then decay rapidly after HF stops (Figure 15b). This also coincides with the seismic events recorded only during HF in Duvernay formation in the deeper region of Fault 1.

For the near or close fault (Fault 2), the seismic events are observed along the fault during and after HF. This corroborates with the CFS values obtained in Figure 16, which shows that CFS values gradually increase

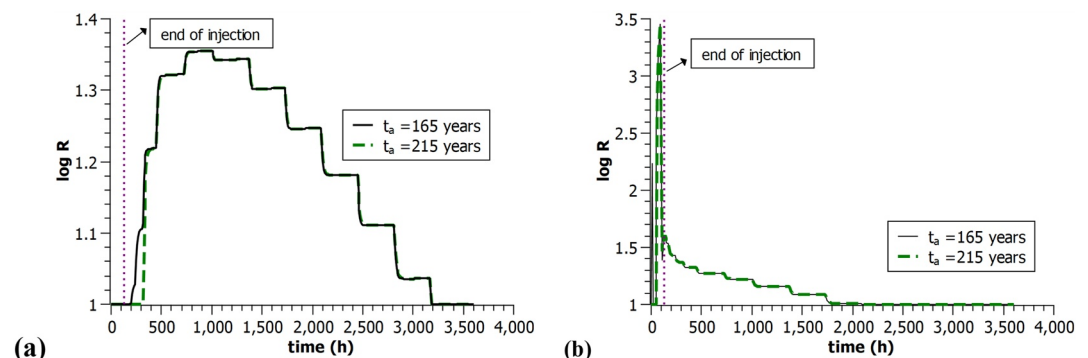


**Figure 15.** The variation with time of  $\log R$  for Fault 1 (distant fault) for the Alberta case (a) for a shallow point and (b) for a deep point on the fault.

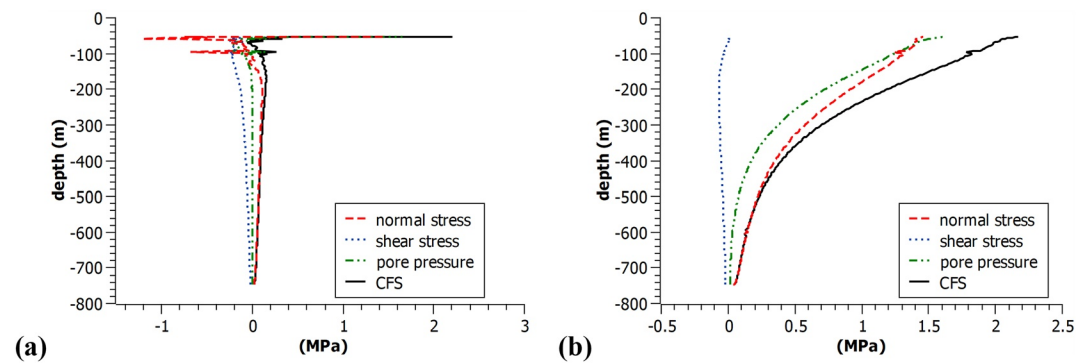


**Figure 16.** Normal and shear stresses, pore pressure, and Coulomb Failure Stress values on Fault 2 (near fault) for the Alberta case (a) during injection (at  $t = 90$  hr), and (b) after injection ends (at  $t = 2,000$  hr).

along the fault in consistency with the expected pore diffusion behavior. The  $\log R$  values for the shallow part (Figure 17a) increase sharply during HF and then decay gradually as pore pressure starts decreasing. For the deep region, the  $\log R$  values (Figure 17b) increase first due to high normal tensile stresses (Figure 16b), and then, as time passes, the pore pressure starts to play a major role as pressure diffuses to the deeper regions resulting in a gradual increase of  $\log R$ .

We note that in the case of Alberta, studies reported that the shale reservoir has an overpressure of 15 kPa/m (Eaton & Schultz, 2018). This overpressure affects the calculation of  $t_a$  as it affects the background effective normal stress. Therefore, we also tested a value of  $t_a$  reduced to 165 years. We compared the  $\log R$  values for  $t_a = 165$  years and  $t_a = 215$  years, and we found no significant changes except in the onset of the increase in the rate of seismicity for the shallow region of Fault 1 (Figure 15a). This means that overpressure can slightly increase the potential for induced seismicity.

## 6. Conclusion

The fault response to stress perturbation from HF is affected by the location of the fault with respect to the HF operations. Based on the assumptions taken in our models, we identify three different responses. For the faults that are close and hydraulically connected to the HF operations, the pore pressure increases rapidly causing an increase in the rate of seismicity or the potential for induced seismicity. For a distant fault, a deformation-induced compressive normal stress stabilizes the upper region of the fault and puts the lower region under extension, which leads to its instability during HF. When the HF operations stop, the rate of seismicity decays. For a fault that is far from the HF operations ( $>2.2$  km), there is no effect of HF on the stability of the fault.

The effect of the other hydrogeological factors like the fault orientation, the width of HF zone, and the injection rate are found to depend on the fault position and the activation mechanism. The fault orientation and damage

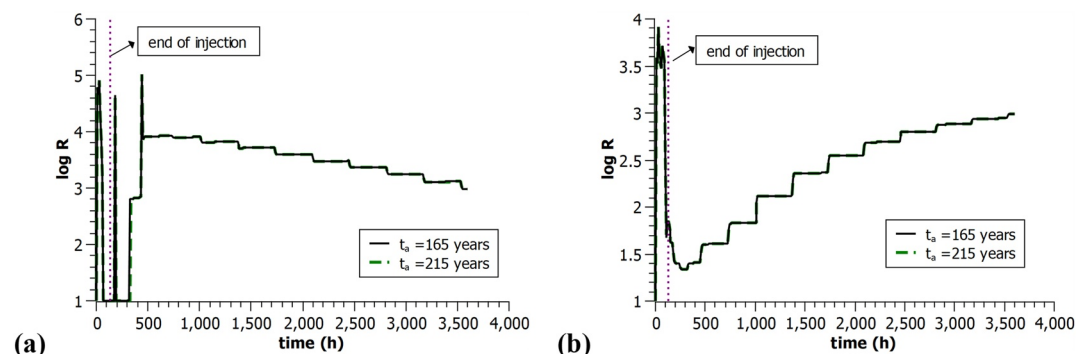


**Figure 17.** The variation with time of  $\log R$  for Fault 2 (near fault) in the Alberta case (a) for a shallow point, and (b) for a deep point on the fault.

zone size only affect the response of the distant fault because the mechanism is dominated by normal and shear stresses. The injection rate has different effects on the fault response and on the potential for induced seismicity depending on how the fault is stressed. If pore pressure is dominant, then reducing the injection rate leads to decreasing the CFS values. However, if normal and shear stresses dominate, then, increasing the injection rate can help stabilize specific regions of the fault. More work should be done on finding optimal injection strategies to avoid induced seismicity by HF.

For the case of HF in the Duvernay formation in Alberta, our results show that the mechanism affecting the distant fault response, during HF, is the shear stress rather than pore pressure diffusion whereas both factors play a role in destabilizing the close fault. The obtained CFS and log  $R$  values correlate with the obtained seismic data in the region, which further reinforces the above findings.

A major assumption taken in our model is the 2D plane strain. The results would differ in a 3D configuration, especially when pressure diffusion is the dominant mechanism. However, even if the magnitude of the change in CFS values differs, we expect to observe the same trends and, thus, make similar conclusions regarding the effect of the studied parameters on induced seismicity from HF.

### Data Availability Statement

The data related to this work can be accessed through the following link: <https://dataverse.harvard.edu/dataset.xhtml?persistentId=doi:10.7910/DVN/2SVLHS>.

### References

- Atkinson, G. M., Eaton, D. W., Ghofrani, H., Walker, D., Cheadle, B., Schultz, R., et al. (2016). Hydraulic fracturing and seismicity in the western Canada sedimentary basin. *Seismological Research Letters*, 87(3), 631–647. <https://doi.org/10.1785/0220150263>
- Bao, X., & Eaton, D. W. (2016). Fault activation by hydraulic fracturing in western Canada. *Science*, 354(6318), 1406–1409. <https://doi.org/10.1126/science.aag2583>
- Basbous, J., Nemer, T. S., Yehya, A., & Maalouf, E. (2022). Assessing the potential for reservoir induced seismicity from the Bisri dam project in Lebanon. *Engineering Geology*, 304, 106679. <https://doi.org/10.1016/j.enggeo.2022.106679>
- Beck, M., Rinaldi, A. P., Flemisch, B., & Class, H. (2020). Accuracy of fully coupled and sequential approaches for modeling hydro- and geomechanical processes. *Comp. Geosci.*, 24(4), 1707–1723. <https://doi.org/10.1007/s10596-020-09987-w>
- Benson, P. M., Austria, D. C., Gehne, S., Butcher, E., Harnett, C. E., Fazio, M., et al. (2020). Laboratory simulations of fluid-induced seismicity, hydraulic fracture, and fluid flow. *Geomechanics for Energy and the Environment*, 24, 100169. <https://doi.org/10.1016/j.gete.2019.100169>
- Biot, M. A. (1941). General theory of three-dimensional consolidation. *Journal of Applied Physics*, 12(2), 155–164. <https://doi.org/10.1063/1.1712886>
- Blanco-Martin, L., Rutqvist, J., & Birkholzer, J. T. (2017). Extension of TOUGH-FLAC to the finite strain framework. *Computers & Geosciences*, 108, 64–71. <https://doi.org/10.1016/j.cageo.2016.10.015>
- TOUGH Symposium 2015: recent enhancements to the TOUGH family of codes and coupled flow and geomechanics processes modeling.
- Bommer, J. J., Oates, S., Cepeda, J. M., Lindholm, C., Bird, J., Torres, R., et al. (2006). Control of hazard due to seismicity induced by a hot fractured rock geothermal project. *Engineering Geology*, 83(4), 287–306. <https://doi.org/10.1016/j.enggeo.2005.11.002>
- Both, J. W., Kumar, K., Nordbotten, J. M., & Radu, F. A. (2018). Anderson accelerated fixed-stress splitting schemes for consolidation of unsaturated porous media. *Computers & Mathematics with Applications*, 77(6), 1479–1502. <https://doi.org/10.1016/j.camwa.2018.07.033>
- Brudzinski, M. R., & Kozłowska, M. (2019). Seismicity induced by hydraulic fracturing and wastewater disposal in the Appalachian Basin, USA: A review. *Acta Geophysica*, 67(1), 351–364. <https://doi.org/10.1007/s11600-019-00249-7>
- Chang, K. W., & Segall, P. (2016). Injection-induced seismicity on basement faults including poroelastic stressing. *Journal of Geophysical Research: Solid Earth*, 121(4), 2708–2726. <https://doi.org/10.1002/2015JB012561>
- Chang, K. W., & Yoon, H. (2018). 3-D modeling of induced seismicity along multiple faults: Magnitude, rate, and location in a poroelasticity system. *Journal of Geophysical Research: Solid Earth*, 123(11), 9866–9883. <https://doi.org/10.1029/2018JB016446>
- Davies, R., Foulger, G., Bindley, A., & Styles, P. (2013). Induced seismicity and hydraulic fracturing for the recovery of hydrocarbons. *Marine and Petroleum Geology*, 45, 171–185. <https://doi.org/10.1016/j.marpetgeo.2013.03.016>
- Davis, C., & Fisk, J. M. (2017). Mitigating risks from fracking-related earthquakes: Assessing state regulatory decisions. *Society & Natural Resources*, 30(8), 1009–1025. <https://doi.org/10.1080/08941920.2016.1273415>
- Deng, F., Dixon, T. H., & Xie, S. (2020). Surface deformation and induced seismicity due to fluid injection and oil and gas extraction in western Texas. *Journal of Geophysical Research: Solid Earth*, 125(5), 1–22. <https://doi.org/10.1029/2019JB018962>
- Deng, K., Liu, Y., & Harrington, R. M. (2016). Poroelastic stress triggering of the December 2013 Crooked Lake, Alberta, induced seismicity sequence. *Geophysical Research Letters*, 43(16), 8482–8491. <https://doi.org/10.1002/2016GL070421>
- De Pater, C. J., & Baisch, S. (2011). Geomechanical study of Bowland Shale seismicity. Synthesis report, 57.
- Dieterich, J. (1994). A constitutive law for rate of earthquake production and its application to earthquake clustering. *Journal of Geophysical Research*, 99(B2), 2601–2618. <https://doi.org/10.1029/93JB02581>
- Eaton, D. W., & Schultz, R. (2018). Increased likelihood of induced seismicity in highly overpressured shale formations. *Geophysical Journal International*, 214(1), 751–757. <https://doi.org/10.1093/gji/ggy167>
- Ellsworth, W. L. (2013). Injection-induced earthquakes. *Science*, 341(6142), 1225942. <https://doi.org/10.1126/science.1225942>
- Fan, Z., Eichhubl, P., & Gale, J. F. W. (2016). Geomechanical analysis of fluid injection and seismic fault slip for the  $M_w$  4.8 Timpson, Texas, earthquake sequence. *Journal of Geophysical Research: Solid Earth*, 3782–3803. <https://doi.org/10.1002/2015JB012608>. Received

### Acknowledgments

The authors would like to thank Pr. James R. Rice, Dr. Tajuldeen Iwalewa, and Dr. Zhuo Yang from Rice Group at Harvard University for the fruitful discussions during the course of this research. The authors would also like to thank the reviewers for their helpful reviews and suggestions. This work is funded by the University Research Board at the American University of Beirut (Award # 103780; Project # 24698).

- Fan, Z., Eichhubl, P., & Newell, P. (2019). Basement fault reactivation by fluid injection into sedimentary reservoirs: Poroelastic effects. *Journal of Geophysical Research: Solid Earth*, 124(7), 7354–7369. <https://doi.org/10.1029/2018JB017062>
- Fisher, K., & Warpinski, N. (2012). Hydraulic-fracture-height growth: Real data. *SPE Production & Operations*, 27(1), 8–19. <https://doi.org/10.2118/145949-pa>
- Frohlich, C. (2012). Two-year survey comparing earthquake activity and injection-well locations in the Barnett Shale, Texas. *Proceedings of the National Academy of Sciences of the United States of America*, 109(35), 13934–13938. <https://doi.org/10.1073/pnas.1207728109>
- Galloway, E., Hauck, T., Corlett, H., Paná, D., & Schultz, R. (2018). Faults and associated karst collapse suggest conduits for fluid flow that influence hydraulic fracturing induced seismicity. *Proceedings of the National Academy of Sciences of the United States of America*, 115(43), E10003–E10012. <https://doi.org/10.1073/pnas.1807549115>
- Gudmundsson, A. (2004). Effects of Young's modulus on fault displacement. *Comptes Rendus Geoscience*, 336(1), 85–92. <https://doi.org/10.1016/j.crte.2003.09.018>
- Gudmundsson, A. (2011). *Rock fractures in geological processes*. Cambridge University Press.
- Gudmundsson, A. (2022). The propagation paths of fluid-driven fractures in layered and faulted rocks. *Geological Magazine*. [https://www.researchgate.net/publication/362226927\\_The\\_propagation\\_paths\\_of\\_fluid-driven\\_fractures\\_in\\_layered\\_and\\_faulted\\_rocks](https://www.researchgate.net/publication/362226927_The_propagation_paths_of_fluid-driven_fractures_in_layered_and_faulted_rocks)
- Healy, J. H., Rubey, W. W., Griggs, D. T., & Raleigh, C. B. (1968). The denver earthquakes. *Science*, 161(3848), 1301–1310. <https://doi.org/10.1126/science.161.3848.1301>
- Holland, A. A. (2013). Earthquakes triggered by hydraulic fracturing in south-central Oklahoma. *Bulletin of the Seismological Society of America*, 103(3), 1784–1792. <https://doi.org/10.1785/0120120109>
- Khadjeh, M., Yehya, A., & Maalouf, E. (2022). Propagation and geometry of multi-stage hydraulic fractures in anisotropic shales. *Geomechanics and Geophysics for Geo-Energy and Geo-Resources*, 8, 124. <https://doi.org/10.1007/s40948-022-00425-y>
- Kim, J. (2010). *Sequential methods for coupled geomechanics and multiphase flow*. PhD thesis. Stanford University.
- Kim, J., Moridis, G., Yang, D., & Rutqvist, J. (2012). Numerical studies on two-way coupled fluid flow and geomechanics in hydrate deposits. *SPE Journal*, 17(02), 485–501. <https://doi.org/10.2118/141304-pa>
- Kleiner, S., & Aniekwe, O. (2019). The Duvernay Shale completion journey. In *Society of Petroleum Engineers: PE Kuwait Oil and Gas Show and Conference 2019, KOGS 2019* (pp. 1–7). <https://doi.org/10.2118/198070-ms>
- McClure, M. W., & Horne, R. N. (2014). Correlations between formation properties and induced seismicity during high pressure injection into granitic rock. *Engineering Geology*, 175, 74–80. <https://doi.org/10.1016/j.enggeo.2014.03.015>
- McGarr, A. (2014). Maximum magnitude earthquakes induced by fluid injection. *AGU: Journal of Geophysical Research: Solid Earth*, 119(2), 3678–3699. <https://doi.org/10.1002/2013JB010597>
- Mendecki, M. J., Szczygiel, J., Lizurek, G., & Teper, L. (2020). Mining-triggered seismicity governed by a fold hinge zone: The Upper Silesian Coal Basin, Poland. *Engineering Geology*, 274, 105728. <https://doi.org/10.1016/j.enggeo.2020.105728>
- Mitchell, T. M., & Faulkner, D. R. (2009). The nature and origin of off-fault damage surrounding strike-slip fault zones with a wide range of displacements: A field study from the Atacama fault system, northern Chile. *Journal of Structural Geology*, 31(8), 802–816. <https://doi.org/10.1016/j.jsg.2009.05.002>
- Peduzzi, P., & Harding, R. (2013). Gas fracking: Can we safely squeeze the rocks? *Environmental Development*, 6(November), 86–99. <https://doi.org/10.1016/j.envdev.2012.12.001>
- Preston, A., Garner, G., & Beavis, K. (2016). Duvernay reserves and resources report.
- Rashedi, H., & Mahani, A. (2016). Data analysis of induced seismicity in Western Canada. *CSEG Recorder*, 2, 26–28.
- Rice, J. R., & Cleary, M. P. (1976). Some basic stress diffusion solutions for fluid-saturated elastic porous media with compressible constituents. *Reviews of Geophysics*, 14(2), 227–241. <https://doi.org/10.1029/RG014i002p00227>
- Rodríguez-pradilla, G. (2018). Reservoir characterization of a Duvernay-Fox Creek shale reservoir using seismic, microseismic, and well log data. *CSEG recorder*, June (pp. 30–34).
- Rutqvist, J. (2011). Stress-versus relationships of fractured rock from in situ experiments and effects of chemical-mechanical coupling. In *AGU Fall Meeting Abstracts, December* (Vol. 2011, p. H53L-04).
- Rutqvist, J., Birkholzer, J., Cappa, F., & Tsang, C. F. (2007). Estimating maximum sustainable injection pressure during geological sequestration of CO<sub>2</sub> using coupled fluid flow and geomechanical fault-slip analysis. *Energy Conversion and Management*, 48(6), 1798–1807. <https://doi.org/10.1016/j.enconman.2007.01.021>
- Rutqvist, J., Rinaldi, A. P., Cappa, F., & Moridis, G. J. (2013). Modeling of fault reactivation and induced seismicity during hydraulic fracturing of shale-gas reservoirs. *Journal of Petroleum Science and Engineering*, 107, 31–44. <https://doi.org/10.1016/j.petrol.2013.04.023>
- Rutqvist, J., Rinaldi, A. P., Cappa, F., & Moridis, G. J. (2015). Modeling of fault activation and seismicity by injection directly into a fault zone associated with hydraulic fracturing of shale-gas reservoirs. *Journal of Petroleum Science and Engineering*, 127, 377–386. <https://doi.org/10.1016/j.petrol.2015.01.019>
- Schultz, R., Stern, V., & Gu, Y. J. (2014). An investigation of seismicity clustered near the Cordell Field, west central Alberta, and its relation to a nearby disposal well. *Journal of Geophysical Research: Solid Earth*, 119(4), 3410–3423. <https://doi.org/10.1002/2013JB010836>
- Schultz, R., Stern, V., Novakovic, M., Atkinson, G., & Gu, Y. J. (2015). Hydraulic fracturing and the Crooked Lake Sequences: Insights gleaned from regional seismic Networks. *Geophysical Research Letters*, 42(8), 261–308. [https://doi.org/10.1007/978-3-319-21314-9\\_8](https://doi.org/10.1007/978-3-319-21314-9_8)
- Schultz, R., Wang, R., Gu, Y. J., Haug, K., & Atkinson, G. (2017). A seismological overview of the induced earthquakes in the Duvernay play near Fox Creek, Alberta. *Journal of Geophysical Research: Solid Earth*, 122(1), 492–505. <https://doi.org/10.1002/2016JB013570>
- Segall, P., & Lu, S. (2015). Injection-induced seismicity: Poroelastic and earthquake nucleation effects. *Journal of Geophysical Research: Solid Earth*, 120(7), 5082–5103. <https://doi.org/10.1002/2015JB012060>
- Stober, I., & Bucher, K. (2014). Hydraulic conductivity of fractured upper crust: Insights from hydraulic tests in boreholes and fluid-rock interaction in crystalline basement rocks. *Crustal Permeability*, 15(1), 161–178. <https://doi.org/10.1111/gfi.12104>
- Suckale, J. (2009). Induced seismicity in hydrocarbon fields. *Advances in Geophysics*, 51, 55–106. [https://doi.org/10.1016/S0065-2687\(09\)05107-3](https://doi.org/10.1016/S0065-2687(09)05107-3)
- Van Eijs, R. M. H. E., Mulders, F. M. M., Nepveu, M., Kenter, C. J., & Scheffers, B. C. (2006). Correlation between hydrocarbon reservoir properties and induced seismicity in the Netherlands. *Engineering Geology*, 84(3–4), 99–111. <https://doi.org/10.1016/j.enggeo.2006.01.002>
- van Thienen-Visser, K., Roholl, J. A., van Kempen, B. M. M., & Muntendam-Bos, A. G. (2018). Categorizing seismic risk for the onshore gas fields in the Netherlands. *Engineering Geology*, 237, 198–207. <https://doi.org/10.1016/j.enggeo.2018.02.004>
- Villarrasa, V., Makhnenko, R., & Gheibi, S. (2016). Geomechanical analysis of the influence of CO<sub>2</sub> injection location on fault stability. *Journal of Rock Mechanics and Geotechnical Engineering*, 8(6), 805–818. <https://doi.org/10.1016/j.jrmge.2016.06.006>
- Villa, V., & Singh, R. P. (2020). Hydraulic fracturing operation for oil and gas production and associated earthquake activities across the USA. *Environmental Earth Sciences*, 79(11), 1–11. <https://doi.org/10.1007/s12665-020-09008-0>

- Walsh, F. R., & Zoback, M. D. (2015). Oklahoma's recent earthquakes and saltwater disposal. *Science Advances*, *1*(5), e1500195. <https://doi.org/10.1126/sciadv.1500195>
- Wang, H. F. (2000). *Theory of linear poroelasticity with applications to geomechanics and hydrogeology*. Princeton University Press.
- Witherspoon, P. A., & Gale, J. E. (1977). Mechanical and hydraulic properties of rocks related to induced seismicity. *Engineering Geology*, *11*(1), 23–55. [https://doi.org/10.1016/0013-7952\(77\)90018-7](https://doi.org/10.1016/0013-7952(77)90018-7)
- Wu, J. H., Liao, C. J., Lin, H. M., & Fang, T. T. (2017). An experimental study to characterize the initiation of the seismic-induced Tsaoiling rock avalanche. *Engineering Geology*, *217*, 110–121. <https://doi.org/10.1016/j.enggeo.2016.12.015>
- Yang, Z., Yehya, A., Iwalewa, T. M., & Rice, J. R. (2021). Effect of permeability evolution in fault damage zones on earthquake recurrence. *Journal of Geophysical Research: Solid Earth*, *126*(9), e2021JB021787. <https://doi.org/10.1029/2021jb021787>
- Yehya, A., & Rice, J. R. (2020). Influence of fluid-assisted healing on fault permeability structure. *Journal of Geophysical Research: Solid Earth*, *125*(10), e2020JB020553. <https://doi.org/10.1029/2020jb020553>
- Yehya, A., Yang, Z., & Rice, J. R. (2018). Effect of fault architecture and permeability evolution on response to fluid injection. *Journal of Geophysical Research: Solid Earth*, *123*(11), 9982–9997. <https://doi.org/10.1029/2018JB016550>
- Zbinden, D., Rinaldi, A. P., Urpi, L., & Wiemer, S. (2017). On the physics-based processes behind production-induced seismicity in natural gas fields. *Journal of Geophysical Research: Solid Earth*, *122*(5), 3792–3812. <https://doi.org/10.1002/2017JB014003>
- Zhao, B. (2018). Geomechanical modelling of induced seismicity. Thesis, August.